MODELLING OF POST-DISRUPTIVE PLASMA LOSS IN THE PRINCETON BETA EXPERIMENT

S.C. JARDIN, J. DELUCIA, M. OKABAYASHI,
N. POMPHREY, M. REUSCH, S. KAYE, H. TAKAHASHI
Princeton Plasma Physics Laboratory,
Princeton University,
Princeton, New Jersey,
United States of America

ABSTRACT. The free-boundary, axisymmetric tokamak simulation code TSC is used to model the transport time-scale evolution and positional stability of the Princeton Beta Experiment (PBX). A disruptive thermal quench will cause the plasma column to move inwards in major radius. It is shown that the plasma can then lose axisymmetric stability, causing it to displace exponentially off the midplane, terminating the discharge. The accuracy of the code is verified by modelling several controlled experimental shots in PBX.

1. INTRODUCTION

The Princeton Beta Experiment (PBX) [1, 2] produces a highly non-circular cross-sectional bean-shaped plasma which enables it to operate at high current and high beta values. A well known consequence of this cross-sectional shaping is the need to provide both passive and active feedback systems [3] to control the axisymmetric instabilities and to maintain the desired cross-sectional shape. In PBX, this is accomplished by three sets of passive aluminium plates connected top-bottom in anti-series, and by active feedback control systems governing both the radial field coils which control the vertical position and the vertical field coils which control the radial position.

The radial position control and the vertical position control are closely coupled in PBX. This coupling, described further in Section 5, is due to the strong radial variation in both the vertical destabilizing force from the external fields and the restoring forces from the passive conductors at fixed locations. The combined system is shown to lose stability if the plasma undergoes a sudden loss of thermal energy or a redistribution of current at high beta, high indentation operation.

The Princeton Tokamak Simulation Code (TSC) [4] is used to model this device. This code was developed to model the axisymmetric transport time-scale evolution and the positional stability and control properties of this tokamak [2] and of other non-circular tokamaks [5–7]. The code is described in detail and is validated against analytic test problems in Ref. [4]. In this paper we first validate the code against experimental data by presenting comparisons with several controlled experimental shots in PBX. We then model a high beta plasma disruption in PBX and show that a small inward radial shift of the plasma, caused either by sudden thermal loss or by decrease of the plasma internal inductance, can cause the system to lose ideal MHD time-scale stability so that the plasma is lost to an axisymmetric mode. This result is in good agreement with the experimental description of disruptive PBX discharges in Ref. [8].

The modelling analysis presented in this paper is largely numerical, being the output of a large complex computer program, TSC. To be credible, we must show that this program can reproduce known results. Verification only against analytic models, as performed in Ref. [4], still leaves open the possibility that the underlying MHD equations, utilized by both the analytic solution and the computer program, provide an inadequate description of the physical experiment. Therefore, comparisons of the code predictions with several controlled experimental shots are presented in Section 2.

2. CODE VERIFICATION

The PBX produces a magnetics data tape for each shot; this tape gives the time history, with millisecond resolution, of the current in each of the three coil systems; the vertical field (VF), the shaping field (SF), the radial field (RF), the plasma current, and the values of the poloidal magnetic flux obtained by integrating the loop voltage at eight flux loop locations. We run

TSC in a predictive mode but use the experimentally measured values of the currents in the three coil systems. We also feedback adjust the rate of flux change from the simulation code Ohmic heating (OH) coil system so that the computed total plasma current agrees with the experimentally measured values at each time point. The 'perfect' OH solenoid used in the code is a good approximation to the actual OH system in PBX, which produces a maximum magnetic field of less than 10 G in the plasma region at full swing.

To test the validity of the simulation model, we then compare the computed values of the poloidal flux at the flux loop locations with the measured values. These values should agree since the code also simulates the induced eddy currents in the adjacent conducting plates and the vacuum vessel. We present the results of several such comparisons.

2.1. Coils only shots

Figures 1–3 show the results of three calibration shots in which an individual coil system was activated but no plasma discharge was initiated. In Fig. 1 the VF system was pulsed (with some inductive coupling to the SF system), while in Figs 2 and 3 the SF and RF systems were activated. Part (d) of Figs 1, 2 and part (c) of Fig. 3 show the flux contours of the magnetic field produced (dotted lines), the location of the experimental flux loops (crosses), the conducting plates, and some of the coils located inside the computational grid. The PBX vacuum vessel and the remaining poloidal field coils are included in the calculation but are not shown. Their locations may be obtained from Ref. [1]. In these runs, the vacuum vessel was modelled as two vertical rows of zones located at R = 0.7 m, $|Z|<0.8$ m, and at R = 2.18 m, $|Z|<0.8$ m. Each 4 cm X 4 cm zone has a resistance of 0.012R ohm.

The passive plates are physically constructed of three up–down pairs of 2.5 cm thick solid aluminium. Each pair is electrically insulated from the other pairs but is connected together in midplane reflection antiseries so that, if a net positive current appears in one plate segment, the same net negative current must appear in its reflection. Each of the six plate segments is modelled with eight to ten computational zones as shown, with the constraint that the net current in each up–down pair of plate segments sum to zero. This construction makes the field penetration time for the radial field much longer than that for the vertical field. Each 4 cm X 4 cm computational zone modelling the conducting plates is given an electrical resistance of r = 0.00064R ohm, where R is the major radius of that zone in metres. The zero net current constraint for plate pairs is imposed in the way discussed in Ref. [4].

Part (a) of Figs 1–3 shows the experimentally measured current traces, which were also used in the

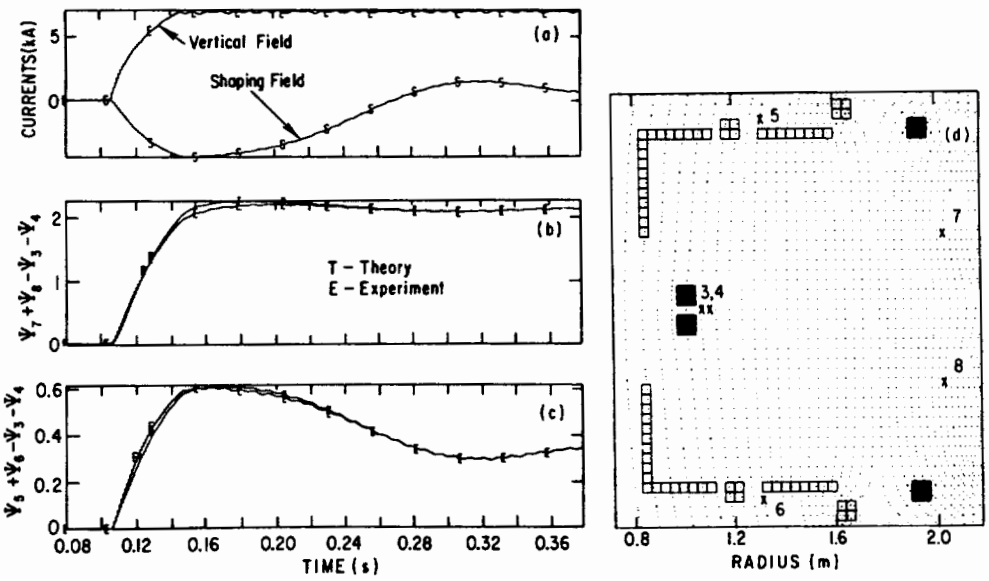

FIG. 1. Vertical field system test without plasma. (a) Experimental currents, (b, c) theoretical (code) and experimental flux differences, (d) flux contours.

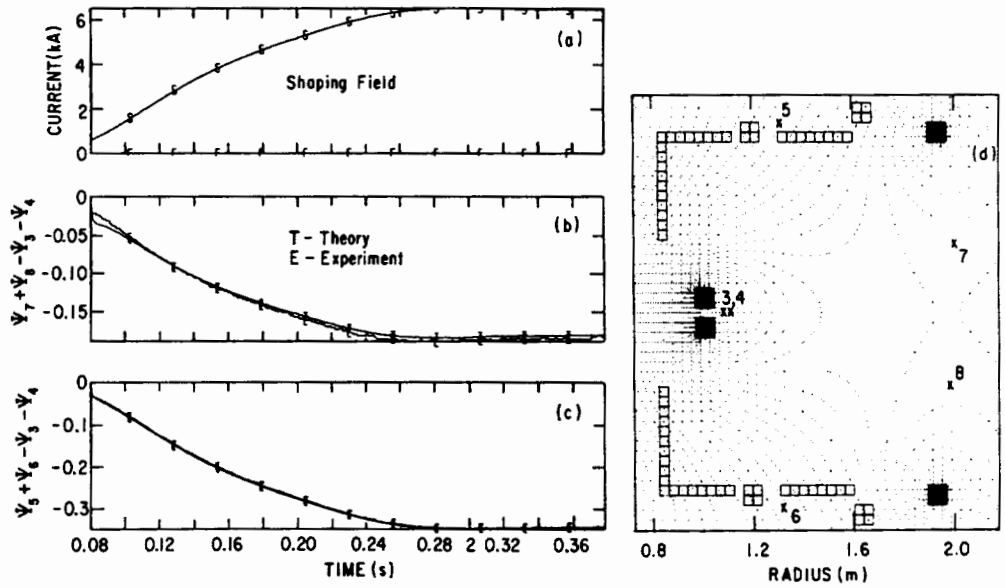

FIG. 2. Shaping field system test without plasma. (a) Experimental currents, (b, c) theoretical (code) and experimental flux differences, (d) flux contours.

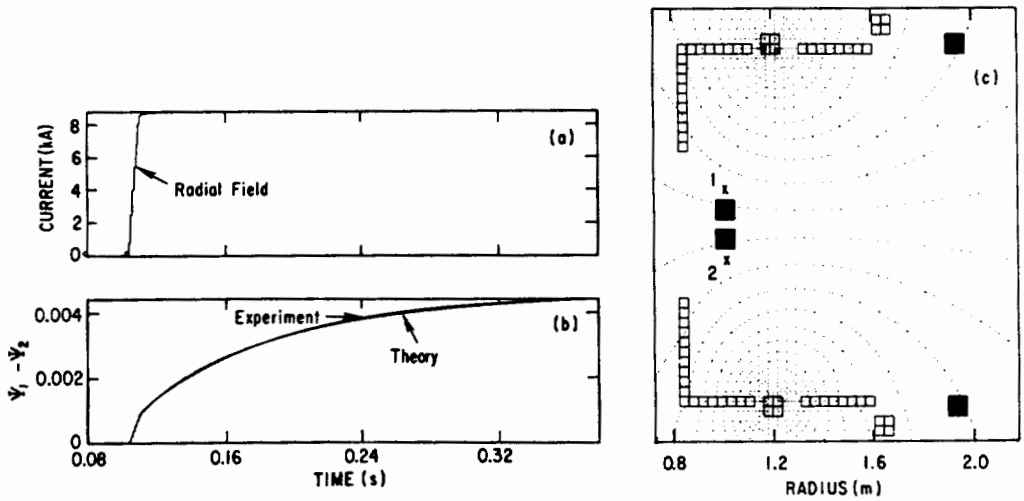

FIG. 3. Radial field system test without plasma. (a) Experimental currents, (b) theoretical (code) and experimental flux differences, (c) flux contours.

calculation. Parts (b) and (c) of Figs 1, 2, and part (c) of Fig. 3 show a comparison between the experimentally measured values and the computed values of certain differences of the poloidal flux at the flux loop locations. The agreement between the theoretical and experimental flux values, as shown in parts (b) and (c) of Figs 1–3, is seen to be quite good. When comparing Figs 1(b) and 3(b) we see that the simulation model is able to reproduce the two-time-scale response of the passive plates quite well. The radial field in Fig. 3 requires several hundred milliseconds to penetrate, while the vertical field in Fig. 1 penetrates in tens of milliseconds.

2.2. Vertical instability

In this controlled experiment, the plasma is held in a bean-shaped configuration, 0.5 cm above the Z = 0 midplane, by adding an offset term to the RF active feedback system. At time t = 0.395 s after plasma initiation, the RF feedback system is short circuited and the plasma displaces vertically off the midplane, with an instability growth time characteristic of the L/R time of the passive aluminium plates.

We model this experiment by running TSC in a predictive mode but using the values of the actual experimental currents in the VF and SF systems, as

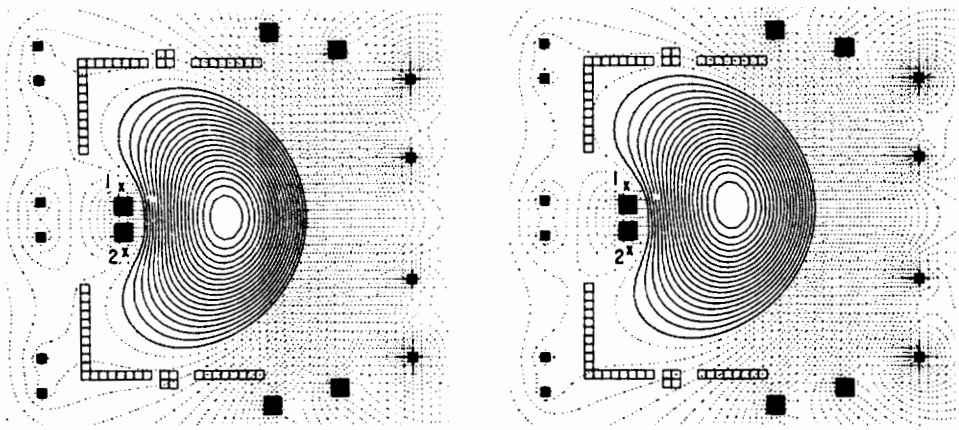

FIG. 4. Magnetic flux contours for the vertical stability test, (a) at the time of feedback shutoff, t = 0.400 s, and (b) at t = 0.475 s.

described in the first paragraph of Section 2. We include active feedback in the RF system and offset the computation feedback system to match the offset currents in the experimental system. The TSC evolves the poloidal and toroidal fields, using a neoclassical resistivity model with $Z_{eff} = 3.0$. The electron and ion temperatures are evolved in time as described in Ref. [4], using the transport model described in the Appendix.

The plasma density is not evolved in time. Rather, we assume a density profile of the form

$$n(\tilde{\psi}, t) = n_0(t)(1 - \tilde{\psi}^{\beta})^{\alpha} + n_b \qquad (1)$$

where $\tilde{\psi}$ is the normalized poloidal flux, which is zero at the magnetic axis and unity at the limiting surface. We adjust $n_0(t)$ to agree with the experimentally measured values of the line averaged density. Values of $\alpha = 1.0, \beta = 2.0, n_b = 4.0 \times 10^{18}$ m^{-3}, give good agreement with density profile measurements.

We begin the simulation at t = 0.30 s. The plasma evolves to a resistive steady state in which magnetic measurements at the eight flux loop locations agree with the experimental values. At time t = 0.395 s the active feedback system in the code is shut off and the resistivity of each of the four computational cells in the feedback coils is set to 0.0003R ohm. The magnetic flux surfaces at the time of feedback shutoff and 75 ms after feedback shutoff are shown in Fig. 4. Figure 5 is a plot of the time history of the flux difference between loops 1 and 2, which is a measure of the vertical displacement. The experimental data for this measurement are also plotted for comparison. The agreement is seen to be quite good.

As a sensitivity test, we have performed another simulation, with the top and bottom horizontal conducting plates moved 4 cm closer to the plasma. The flux difference plot for this run, also shown in Fig. 5, is substantially different from the original simulation and the experimental curves. We can conclude that the simulation program can adequately resolve this difference between plate locations.

The TSC uses an 'enhanced mass technique' to deal with the severe time-scale discrepancy between ideal wave-like phenomena and resistive diffusion-like phenomena in a tokamak. As described in Ref. [4],

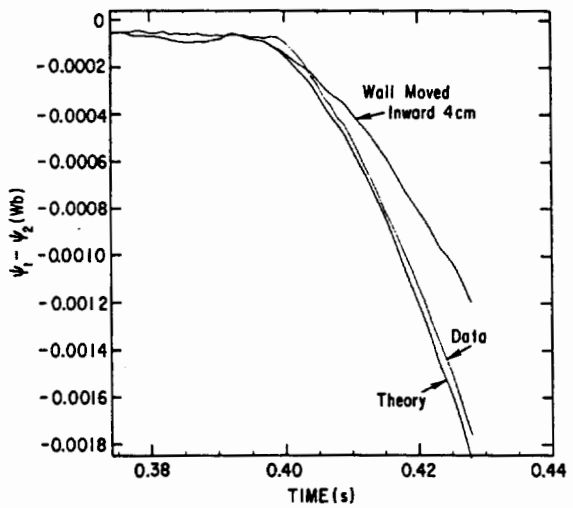

FIG. 5. Comparison of simulation (theory) and experimental values for the flux difference between loops 1 and 2. Also shown is a curve for a calculation performed with top and bottom plates moved 4 cm closer to the plasma.

this is equivalent to adding a fictitious viscous term and increasing the ion mass by a large mass enhancement factor, typically several thousand. Normal resistive evolution and resistive time-scale instabilities should be independent of this factor, while ideal time-scale instabilities should exhibit growth rates proportional to the square root of this factor. Thus, as a second sensitivity test, we repeated this simulation, with the mass enhancement factor reduced by a factor of four and with the artificial viscosity parameter reduced by a factor of two. The curves from these runs coincide with the original curves, confirming that the instability is on a resistive time-scale as opposed to an ideal MHD time-scale and that the code is adequately converged in these parameters.

3. POST-DISRUPTIVE PLASMA LOSS

The major disruption in a tokamak is observed to occur in two phases, known as the thermal quench phase and the current decay phase. The thermal quench phase is nearly instantaneous on the MHD time-scale, lasting only about 50 μs on PBX. During this time, the plasma is observed to lose more than three quarters of its thermal energy because of some enhanced transport mechanism such as magnetic island overlap. The sudden reduction of temperature leads to the much slower current decay phase in which the plasma current decays in a few milliseconds because of the greatly increased plasma resistivity. The axisymmetric dynamics of this second phase is thought to be correctly described by MHD if the enhanced plasma resistivity and the adjacent conducting structures are taken into account.

We start by modelling the plasma evolution during the stable phase of the discharge. To model the plasma disruption, we 'mock up' the thermal quench phase by suddenly increasing the plasma thermal diffusion coefficient to a value significantly above its non-disruptive level. We then compute the axisymmetric dynamics of this new decreased beta configuration, in particular evaluating its vertical stability properties.

3.1. High beta stable evolution

We used the TSC to simulate the axisymmetric evolution of a high beta discharge in PBX. The currents in the SF and VF coil systems were taken from the experimental data tape for shot No. 95737. The total plasma current I_p and the central density n_0 were adjusted to match the experimental values in the same way as described in Section 2.2. In this run the mid-plane line integral density increased nearly linearly from 1.3×10^{19} at t = 0.25 s to 2.6×10^{19} at t = 0.55 s. We again utilized the anomalous transport model described in the Appendix. A Z_{eff} value of 3.0 was used to match the value obtained from spectroscopy.

To model the neutral beam injection, we take the ion energy source deposition profile to be a function of the normalized poloidal flux $\tilde{\psi}$:

$$S^E(\tilde{\psi}, t) = S_0^E(t) \left[\left(\frac{(\tilde{\psi} - a)^2 + d^2}{d^2} \right) (1 - \tilde{\psi})^2 \right] \qquad (2)$$

where a = 0.1, d = 0.5, and the normalization factor $S_0^E(t)$ is prescribed to give 1.1 MW injection at t = 0.36 s, 2.2 MW at t = 0.41 s, 3.4 MW at t = 0.44 s, and 4.5 MW at t = 0.52 s (see Fig. 8).

The toroidal currents in the coil systems and in the plasma are shown in Fig. 6 as a function of time. Fig. 7(a) is a plot of the flux differences between the flux loop values $(\psi_3 + \psi_4)$ and $(\psi_7 + \psi_8)$ (upper curves), and between $(\psi_3 + \psi_4)$ and $(\psi_5 + \psi_6)$ (lower curves). The good agreement between the computed and measured values of the upper curves of flux loop values was facilitated by allowing the simulation code to adjust a multiplier, f_m, in front of the anomalous electron thermal transport coefficient, as described in the Appendix. The value of f_m used in the simulation

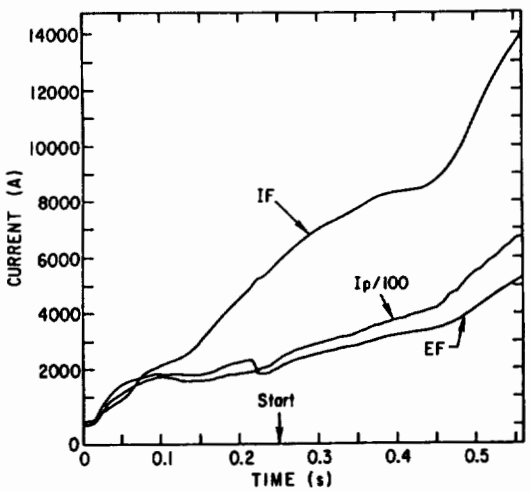

FIG. 6. Currents in VF and IF (or SF) coil systems, and plasma currents as a function of time, in experiment and simulation for high beta shot No. 95737.

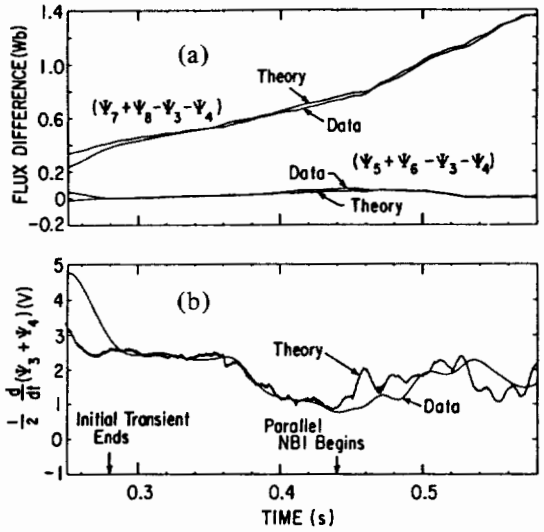

FIG. 7. Comparison of experimental and computational flux differences for high beta shot No. 95737, measuring (a) radial position (upper curves) and indentation (lower curves), and (b) loop voltage average for flux loops 3 and 4.

varied between 0.6 and 1.8, as shown in Fig. 8. The computed loop voltage, defined as the average of the time derivative of two flux loop values, $(1/2)\ \mathrm{d}/\mathrm{dt}\ (\psi_3 + \psi_4)$, is shown in Fig. 7(b) together with the experimental value.

It is remarkable how well both of the computed flux loop differences of Fig. 7 agree with their respective experimental values. Even with the upper curve agreement being facilitated by adjusting the multiplier f_m as shown in Fig. 8, the comparison of the lower curves in Fig. 7(a) and the loop voltage in Fig. 7(b) represents a sensitive test of the current distribution and penetration, and of the plasma resistivity and hence the transport model used.

It is interesting to note how well the computed loop voltage in Fig. 7(b) agrees with the measured value, in particular in the time period $0.30 < t < 0.44$. Although the plasma current increases from 300 kA to 400 kA in this period, the loop voltage differs by only a few per cent. The difference between the theoretical and experimental loop voltage curves in the initial time period $0.25 < t < 0.28$ is not significant, being due only to a rather bad choice for the initial equilibrium current distribution. As the plasma profiles evolve in time according to the transport equations in TSC, the dependence of the curves on the initial conditions diminishes, and the theoretical and experimental curves begin to match after about 30 ms, which is comparable to the energy confinement time.

Of more physical significance is the disagreement between the theoretical and experimental loop voltage curves in the time period $0.44 < t < 0.58$. This is the time period over which the two neutral beam injectors oriented parallel to the magnetic field were activated. A separate analysis of this shot by the TRANSP code shows that these high energy injected particles carry of the order of ten per cent of the total plasma current. Since our plasma resistivity model makes no attempt to simulate highly non-thermal current carriers, we expect the theoretical and experimental curves to differ in this time span. Nevertheless, it is interesting to note that the loop voltage curves agree during the perpendicular injection phase but not during the parallel injection. A more detailed accounting of this discrepancy is deferred to a future publication.

3.2. Axisymmetric instability

To model a disruptive thermal quench, we abruptly increase the transport multiplier f_m at time $t = 0.566$ s from 0.6 to a value in the range 0.8–2.0. The plasma beta reduces accordingly and the plasma comes into a new equilibrium with the same total current at a decreased value of major radius, with its magnetic axis in the range $R = 1.34$–1.44 m. The vertical feedback system is turned off and the passive plate resistivity is reduced to zero. The vertical offset of the plasma, which had been held at 0.5 cm above the midplane by the active feedback system, is observed as a function

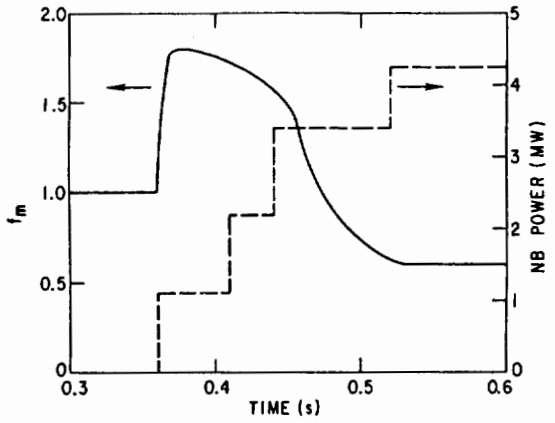

FIG. 8. Neutral beam power and transport multiplier applied in the simulation of the high beta shot.

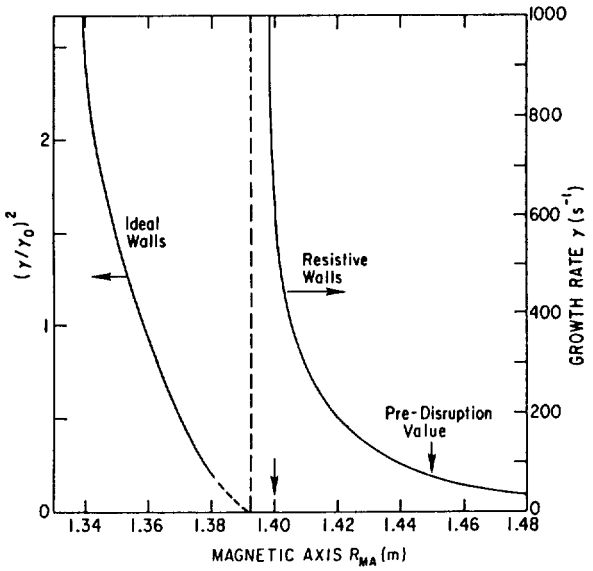

FIG. 9. Scaled growth rate for ideal time-scale axisymmetric instability (left) and for resistive time-scale growth rate (right), as a function of magnetic axis position at full current, with high beta operation. The active feedback system is turned off to generate these curves.

of time. If the passive plates are not sufficient to provide ideal time-scale stability, the Z-position of the plasma magnetic axis will exhibit exponential growth, otherwise it will oscillate in time, indicating stability.

The results of this study are summaraized in Fig. 9, which is a plot of the square of the unstable growth rate for the vertical instability as a function of the new radial position of the magnetic axis after the thermal quench. The stability boundary for axisymmetric displacement is seen to be approximately R = 1.39 m, which corresponds to a decrease in beta from 4% to 3%. If the plasma is displaced to a magnetic axis position smaller than R = 1.39 m, the discharge will be lost to a vertical motion.

Also shown in Fig. 9 is the computed growth rate of the resistive time-scale axisymmetric mode, using the true value of the passive plate resistivity. This mode only exists in the region of magnetic axis location that is stable for zero plate resistivity. This curve was obtained in the same manner as described above, except that the passive plate resistivity was not changed from its original value when the transport multiplier was increased.

We see that the finite resistivity mode has a pole at the ideal stability boundary R ≅ 1.39 m. This is consistent with the simple scaling [3]

$$\gamma = \gamma_R \frac{\gamma_0^2}{\gamma_s^2 - \gamma_0^2} \tag{3}$$

where γ_R is the inverse L/R decay time of the plates, γ_0 is the ideal MHD growth rate if no walls are present, and γ_s measures the stabilizing effect of the plates if they are perfectly conducting.

The resistive time-scale growth rate increases rapidly as the plasma radius decreases from the pre-disruptive value of R = 1.45 m to the ideal stability boundary at R = 1.39 m. At some value of major radius in the range $1.39 < R < 1.45$, the active feedback system clearly becomes inadequate and the axisymmetric stability will be lost, even though the system has ideal MHD stability.

A typical unstable sequence is presented in Fig. 10, showing (a) a high beta plasma equilibrium which in (b) is displaced to a smaller major radius because of a disruptive thermal quench and in (c) is displaced exponentially off the midplane because of axisymmetric instability.

Figure 11 shows a comparison of the time histories of the poloidal field during the last six milliseconds, as

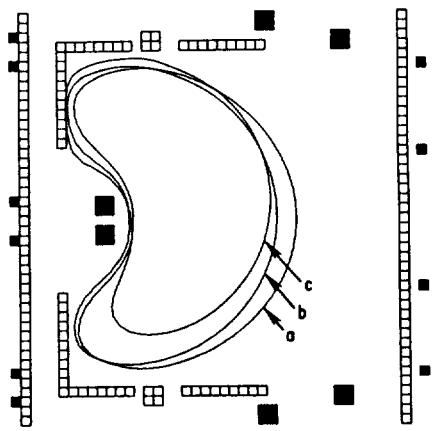

FIG. 10. Plasma flux surfaces at three times, showing an unstable sequence. (a) High beta plasma suffers a thermal quench, causing it to move inwards in major radius to a position where it is unstable to axisymmetric instability (b) and displaces off the midplane (c), causing discharge termination.

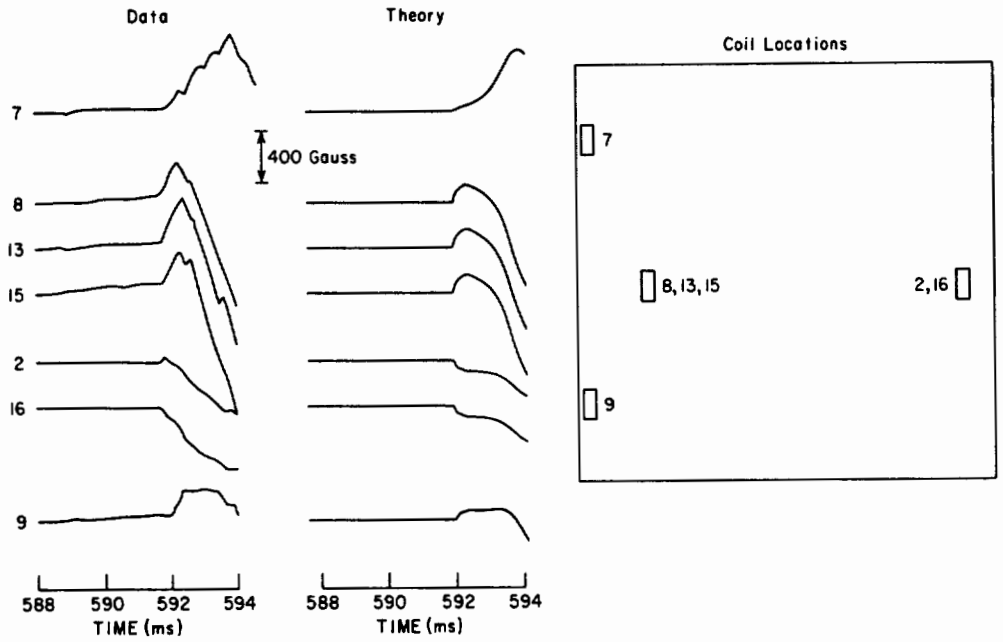

FIG. 11. Comparison of measured and computed magnetic fields at Mirnov coils for the disruption phase of PBX shot No. 95732.

measured by seven Mirnov coils and computed for PBX shot No. 95732. This shot is virtually identical with the previously discussed shot No. 95737, but Mirnov coil data are available for this time period. The coil locations are indicated in the figure and described further in Ref. [8]. We note here that coils 8, 13 and 15 are in the same poloidal location but are rotated toroidally 120° from each other; the same is true for coils 2 and 16, the orientation of which is opposite to that of the other coils. The computed fields in each of these coil sets will always be identical since the computation assumes axisymmetry. The fact that the measured values are nearly identical for each coil set indicates that the discharge termination is nearly axisymmetric for this shot.

To model the disruptive event, we increased the thermal transport coefficients at t = 592 ms to cause the plasma beta to suddenly decrease from 4% to 2% in 0.5 ms. The plasma shifts inwards in major radius to a magnetic axis position of approximately 140 cm. A small initial vertical offset (0.5 cm in the simulation) causes the plasma to displace upwards, as shown in Fig. 10, and by t = 594 ms the plasma decays in the upper left corner of the vacuum vessel.

From a comparison of the experimental and theoretical traces in Fig. 11, it can be concluded that there is good qualitative agreement between the simulation and the experimental data. The experimental traces clearly exhibit a radial contraction phase in which the plasma moves inwards. This is shown during the first 0.5 ms by an increase in all loops except for the outboard loops 2 and 16, which decrease. In the next phase, lasting approximately 2 ms, loops 8, 13 and 15 decrease while loop 7 increases as the plasma is displaced vertically upwards. Finally, all loops decrease as the plasma current is quenched. From the stability diagram in Fig. 9 and from the slopes and amplitudes of the Mirnov measurements in Fig. 11 we see that the plasma never became ideal MHD unstable but was lost because of an axisymmetric instability whose growth rate scales with the wall resistivity. An ideal time-scale instability would appear instantaneous, or as a vertical line on this time-scale.

4. SUMMARY AND CONCLUSIONS

We have demonstrated that the vertical instability is an important factor present in the high beta operation

of PBX. The plasma is stable during normal high beta operation, but small departures from this normal operation, such as the major radius shift associated with the thermal quench phase of the plasma disruption, will cause loss of axisymmetric stability. It is also possible, as speculated in Ref. [8], that slight inward radial excursions due to large sawtooth oscillations at high beta, high indentation operation are sufficient to cause the plasma to lose axisymmetric stability.

It is significant in itself that PBX is able to operate in a stable manner so close to the instability boundary. This demonstration should have an impact on the design of other non-circular tokamaks. We can conclude that precision design of tokamaks relying on conducting walls for ideal time-scale stability is now warranted, but that knowledge of only the ideal MHD axisymmetric stability boundary is not sufficient to guarantee stability. It is necessary to evaluate the growth rates of modes that depend on finite wall resistance near the ideal MHD stability boundaries.

The comparison of the TSC predictions with controlled experimental calibration runs described in Section 2 gives credibility to the numerical simulation results presented in Section 3. In addition, we believe that the simulation program TSC should prove of value in the interpretation of data from other existing experiments as well as in the planning and modification of new experiments.

Appendix

TRANSPORT MODEL

In the simulations presented in this paper, we use a two-regime anomalous transport model with neoclassical resistivity. The model is a modification of Tang's [9] profile-consistent microinstability model to general axisymmetric geometry.

We take the electron thermal conductivity to be of the form [10]

$$\chi_e = f_m \left| (\chi^0_{OH})^2 + (\chi^0_{AUX})^2 \right|^{1/2} F(\Phi) \qquad \text{(A-1)}$$

where the form factor $F(\Phi)$ is

$$F(\Phi) = \frac{n_e(0)}{n_e(\Phi)} \frac{P(\Phi)}{P(\Phi_0)} 8\pi^2 \frac{\Phi_0 R}{(dV/d\Phi)\,|\nabla\Phi|^2} \times \exp\left(\frac{(2/3)\alpha_q \Phi}{\Phi_0}\right) \qquad \text{(A-2)}$$

Here, Φ is the toroidal magnetic flux, equal to Φ_0 at the plasma edge, $P(\Phi)$ is the heating power (Ohmic plus auxiliary) inside the surface Φ, $n_e(\Phi)$ is the electron density profile given by Eq. (1), R is the major radius of the magnetic axis, $V(\Phi)$ is the flux surface volume, and α_q is taken to be

$$\alpha_q = q_e + 0.5 \qquad \text{(A-3)}$$

where q_e is the safety factor at the surface containing 90% of the toroidal flux between the magnetic axis and the plasma–vacuum interface. From Ref. [9] we obtain for the two confinement regimes in Eq. (A-1)

$$\chi^0_{OH} = \frac{4.0}{n_e(0)} \frac{a(RB_T)^{0.3} Z_{eff}^{0.2}}{R^{2.2} q_e^{1.6}} \qquad \text{(A-4)}$$

$$\chi^0_{AUX} = (0.09)\left[\frac{P(\Phi)}{n_e(0)}\right]^{0.6} \frac{1}{(RB_T q_a)^{0.8} a^{0.2}} \qquad \text{(A-5)}$$

where a is the average minor radius and B_T is the vacuum toroidal field strength on axis. All quantities are MKS, except for the power P(MW) and the central electron density, $n_e(0)$ (10^{20} m^3).

The multiplier f_m is constrained to be unity before the neutral beams are turned on; then it varies in the range 0.6–1.8, as shown in Fig. 8. We take the ion thermal conductivity to be equal to the electron value given by Eq. (A-1).

A general geometry generalization of the neoclassical resistivity of Ref. [11] was used, with the calculation of the particle trapping fraction taken from Ref. [12] and the resistivity inside the q = 1 surface set equal to the value at this surface.

ACKNOWLEDGEMENTS

The authors are indebted to colleagues from the PBX group for making their data freely available, and for co-operation and encouragement in the analysis of these data. The help of Drs. P. Couture and R. Fonck should be specially mentioned. Useful discussions with Drs. A.H. Boozer, M. Redi and W.M. Tang are also acknowledged.

This work was supported by the United States Department of Energy, under Contract No. DE-AC02-76-CHO-3073.

REFERENCES

[1] BOL, K., CHANCE, M., DEWAR, R., The Princeton Beta Experiment PBX, Rep. PPPL-2032, Princeton Plasma Physics Laboratory (1983).
[2] OKABAYASHI, M., BEIERSDORFER, P., BOL, K., BUCHENAUER, D., CHANCE, M.S., et al., in Plasma Physics and Controlled Nuclear Fusion Research 1984 (Proc. 10th Int. Conf. London, 1984), Vol. 1, IAEA, Vienna (1985) 229.
[3] JARDIN, S.C., LARABEE, D., Nucl. Fusion **22** (1982) 1095.
[4] JARDIN, S.C., POMPHREY, N., DELUCIA, J.L., J. Comput. Phys. **66** (1986) 481.
[5] MARCUS, F., JARDIN, S., HOFFMANN, F., Phys. Rev. Lett. **55** (1985) 2289.
[6] MIDZUNO, Y., BELL, M., DELUCIA, J.L., JARDIN, S.C., POMPHREY, N., TANG, W.M., Bull. Am. Phys. Soc. **30** (1985) 1524.
[7] MERRILL, B., JARDIN, S.C., DSTAR: A comprehensive tokamak resistive disruption model for vacuum vessel components, to be published in Nucl. Eng. Des./Fusion.
[8] ITAMI, K., JAHNS, G., YAMADA, H., McGUIRE, K., Classification of Disruption in PBX, Rep. PPPL-2260, Princeton Plasma Physics Laboratory (1985).
[9] TANG, W.M., Nucl. Fusion **26** (1986) 1605.
[10] GOLDSTON, R., Plasma Phys. Controll. Fusion **26** (1986).
[11] HIRSHMAN, S., HAWRYLUK, R., Nucl. Fusion **17** (1977) 611.
[12] HIRSHMAN, S., JARDIN, S.C., Phys. Fluids **22** (1979) 731.

(Manuscript received 25 June 1986
Final manuscript received 18 November 1986)